Interpretable Machine Learning based Detection of Coeliac Disease

F. Jaeckle[*,1, 2], R. Bryant[*,1], J. Denholm,[1, 2, 3] J. Romero Diaz[1,2], B. Schreiber[1,3], V. Shenoy[1], D. Ekundayomi[1], S. C. Evans[1], M. J. Arends[4], and E. Soilleux[1, 2]

[1]Department of Pathology, University of Cambridge, Tennis Court Road, CB2 1QP, Cambridge, England, UK.

[2]Lyzeum Ltd, Cambridge, CB1 2LA, England, UK.

[3]Department of Applied Mathematics and Theoretical Physics,

University of Cambridge, Wilberforce Road, CB3 0WA, Cambridge, England, UK.

[4]University of Edinburgh, Division of Pathology, Edinburgh Cancer Research UK Cancer Centre, Institute of Genetics and Molecular Medicine, Edinburgh EH4 2XR, Scotland, UK.

Abstract

Background: Coeliac disease, an autoimmune disorder affecting approximately 1% of the global population, is typically diagnosed on a duodenal biopsy. However, inter-pathologist agreement on coeliac disease diagnosis is only around 80%. Existing machine learning solutions designed to improve coeliac disease diagnosis often lack interpretability, which is essential for building trust and enabling widespread clinical adoption.

Objective: To develop an interpretable AI model capable of segmenting key histological structures in duodenal biopsies, generating explainable segmentation masks, estimating intraepithelial lymphocyte (IEL)-to-enterocyte and villus-to-crypt ratios, and diagnosing coeliac disease.

Design: Semantic segmentation models were trained to identify villi, crypts, IELs, and enterocytes using 49 annotated 2048x2048 patches at 40x magnification. IEL-to-enterocyte and villus-to-crypt ratios were calculated from segmentation masks, and a logistic regression model was trained on 172 images to diagnose coeliac disease based on these ratios. Evaluation was performed on an independent test set of 613 duodenal biopsy scans from a separate NHS Trust.

Results: The villus-crypt segmentation model achieved a mean PR AUC of 80.5%, while the IEL-enterocyte model reached a PR AUC of 82%. The diagnostic model classified WSIs with 96% accuracy, 86% positive predictive value, and 98% negative predictive value on the independent test set.

Conclusions: Our interpretable AI models accurately segmented key histological structures and diagnosed coeliac disease in unseen WSIs, demonstrating strong generalization performance. These models provide pathologists with reliable IEL-to-enterocyte and villus-to-crypt ratio estimates, enhancing diagnostic accuracy. Interpretable AI solutions like ours are essential for fostering trust among healthcare professionals and patients, complementing existing black-box methodologies.

[*] These authors contributed equally to this manuscript.

What is already known on this topic:

Pathologist concordance in diagnosing coeliac disease from duodenal biopsies is consistently reported to be below 80%, highlighting diagnostic variability and the need for improved methods. Several recent studies have leveraged artificial intelligence (AI) to enhance coeliac disease diagnosis. However, most of these models operate as "black boxes," offering limited interpretability and transparency. The lack of explainability in AI-driven diagnostic tools prevents widespread adoption by healthcare professionals and reduces patient trust.

What this study adds:

This study presents an interpretable semantic segmentation algorithm capable of detecting the four key histological structures essential for diagnosing coeliac disease: crypts, villi, intraepithelial lymphocytes (IELs), and enterocytes. The model accurately estimates the IEL-to-enterocyte ratio and the villus-to-crypt ratio, the latter being an indicator of villous atrophy and crypt hyperplasia, thereby providing objective, reproducible metrics for diagnosis. The segmentation outputs allow for transparent, explainable decision-making, supporting pathologists in coeliac disease diagnosis with improved accuracy and confidence.

How this study might affect research, practice or policy:

This study presents an AI model that automates the estimation of the IEL-to-enterocyte ratio—a labour-intensive task currently performed manually by pathologists in limited biopsy regions. By minimising diagnostic variability and alleviating time constraints for pathologists, the model provides an efficient and practical solution to streamline the diagnostic workflow. Tested on an independent dataset from a previously unseen source, the model demonstrates explainability and generalizability, enhancing trust and encouraging adoption in routine clinical practice. Furthermore, this approach could set a new standard for AI-assisted duodenal biopsy evaluation, paving the way for the development of interpretable AI tools in pathology to address the critical challenges of limited pathologist availability and diagnostic inconsistencies.

I. Introduction

With the emergence of digital pathology, artificial intelligence (AI) has the potential to improve the accuracy and speed of diagnosis. Duodenal (small intestinal) biopsies in particular are well suited to develop novel AI algorithms for, as the percentage of malignant diagnoses (<1%) is small compared to other parts of the body.

The most common pathology found in the duodenum is coeliac disease, a chronic autoimmune disorder triggered by the ingestion of gluten, a protein found in barley, wheat and rye (1). It is estimated to affect approximately 1% of the global population, with significant regional variations (2,3). The only available treatment is following a life-long gluten-free diet.

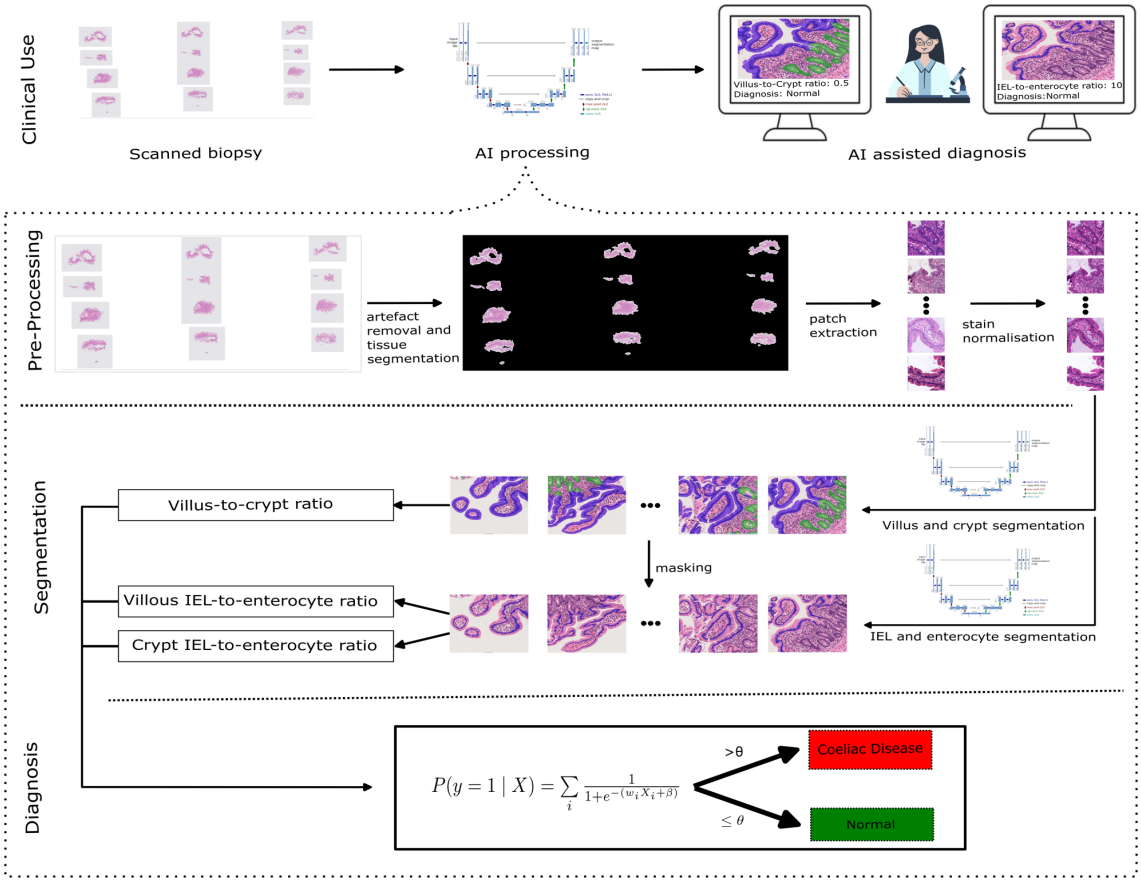

Figure 1. Model pipeline: *The pipeline consists of the following steps: i) artefacts are removed, and the tissue is selected; ii) the tissue is divided into small patches. iii) stain normalisation is applied.; iv) villi and crypts are segmented using a U-Net model; v) IELs and enterocytes are segmented within the already segmented villi and crypts using another U-Net model; vi) the villus-to-crypt ratio and IEL-to-enterocyte ratios in both villi and crypts are computed; vii) a simple logistic classification model diagnoses the sample as either coeliac disease or normal. The outputs, including segmentation masks, the computed ratios, and the final diagnosis, are presented to a pathologist for review.*

Coeliac disease can lead to variety gastrointestinal and systemic symptoms including vitamin deficiency, anaemia, weight loss, diarrhoea, fatigue, and infertility (4). Furthermore, if left untreated it can significantly increase the risk of developing duodenal adenocarcinoma and lymphoma (6,7).

Current diagnosis: Most guidelines suggest a serological test for patients with symptoms suggestive of coeliac disease. Unless the level of the tTG-IgA antibody count is exceeding 10 times the normal value and IgA EMA test positive in a second blood sample, a duodenal biopsy is recommended as the gold standard for coeliac disease diagnosis (8–10). Pathologists diagnose coeliac disease on microscopic sections of duodenal biopsies viewed under the microscope or as a scanned image, by identifying a number of

abnormalities. These include an increased ratio of intraepithelial lymphocytes (IELs) to enterocytes in the villi, villous atrophy (significant blunting and reduction in size of the villi, sometimes to a flat appearance), and crypt hyperplasia (crypts becoming longer and thinner) (11). However, a number of independent studies have showed the agreement between pathologists when diagnosing coeliac disease to be lower than 80% (11–21), underlining the unmet clinical need for a more accurate diagnostic solution.

Other work in this area: Several recent studies have aimed to improve the diagnosis of coeliac disease on H&E-stained biopsies with AI. The majority used black-box classification algorithms that output a single diagnosis without providing any explanations or justifications which provides a significant barrier towards adoption. Furthermore, most of studies did not test their models on an independent test set which would provide insights into its robustness and ability to handle common variability in image acquisition and staining procedures.

Wei et al. (22) trained a convolutional neural network (CNN) to classify individual 224x224 pixel patches as coeliac disease, normal, or non-specific duodenitis, achieving accuracies or 95.3%, 91.0%, and 89.2% respectively. However, they did not test their algorithm on an independent test set from a different source.

Sali et al. (23) trained a model to predict the Marsh-Oberhuber classification (24,25), an algorithm that classifies biopsies into different classes of coeliac disease severity. However, the study only included images from 34 patients.

Seyd et al. (26) developed a machine learning model to diagnose coeliac disease, environmental enteropathy (EE), and normal cases. However, the authors used different types of input images: EE images were digitized slides, whereas the coeliac disease and normal images were taken from a microscope at different resolutions. It is therefore possible that the model simply learned the image type rather than any pathological features.

Koh et al. (27) proposed a machine learning algorithm based on Steerable Pyramid Transform and entropy features to detect coeliac disease and classify its severity using Marsh scores. The most significant limitations of this study are the small size of the dataset and the lack of external validation on a dataset from a different source.

Kowsari et al. (28) proposed a hierarchical medical image classification (HMIC) approach using multiple deep learning models to classify small bowel enteropathies hierarchically. The model achieved high accuracy in classifying EE, coeliac disease, and normal controls, as well as coeliac disease severity. While promising, the study relied on a limited dataset from a single institution, which may not be representative of the broader patient population.

Tabacchi et al. (29) developed a Clinical Decision Support System (CDSS) for aiding in the diagnosis of coeliac disease. The system, named ITAMACDSS, employed a fuzzy

classifier based on neural networks. The main weakness of the paper is that the test set is small (n=20) and comes from the same source as the training set.

Denholm et al. (30) trained a CNN using multiple-instance-learning to diagnose WSIs as normal or coeliac disease. The main limitation of this study is that it includes only clear cases of coeliac disease and normal duodenal mucosa and no ambiguous cases or images with different diagnoses which limit its real-life impact.

A few recent studies have attempted to use image segmentation techniques to diagnose coeliac disease in a more explainable manner.

Gruver et al. (31) used a customizing off-the-shelf AI software to segment villous epithelium, lamina propria, and crypts on H&E stained biopsies and IELs and enterocytes on CD3 immunohistochemistry WSIs. The two main drawbacks are firstly that the cell detection is carried out on CD3 stained biopsies which are rarely used in routine reporting practice and secondly the algorithm is trained and tested on images from the same source, therefore not proving any generalisation performance.

Griffin et al. (32) created a CNN to identify cells, tissue, and artifact regions in biopsies of celiac disease and normal duodenal tissue. They extracted features from these regions and correlated them with Marsh scores. Weaknesses of their approach are the small size of the test set (n=28) and that the test set cases came from the same source as the training images.

In this study we developed an explainable model for the interpretable analysis of duodenal biopsies and the accurate diagnosis of coeliac disease. We summarise our main contributions as follows:

1. We trained segmentation models for duodenal biopsies that detect villi, crypts, enterocytes, and intraepithelial lymphocytes (IELs).
2. We used the model outputs to accurately predict the IEL-to-enterocyte ratio in duodenal biopsies, a key indicator for diagnosing coeliac disease.
3. We further use the model outputs to predict the villus-to-crypt ratio, that acts as a close approximation to the level of villous atrophy and crypt hyperplasia.
4. We trained a logistic regression classifier that takes as input the IEL-to-enterocyte and villus-to-crypt ratios and outputs an accurate coeliac disease diagnosis on a set of representative biopsies from a new source.

The strong generalisation performance and the interpretable nature of our model outputs increases the likelihood of clinical adoption.

II. Data

Segmentation training dataset: We trained our segmentation models on 49 annotated patches at 40x magnification (approximately 0.25 microns per pixel), each sized 2024x2024 pixels, to ensure they were sufficiently large to be able to include multiple villi.

The patches are taken from 43 unique WSIs from five different medical centres scanned using four different scanners (see Table S1). 27 patches come from images with a previous normal diagnosis, 15 from coeliac disease WSIs, and 7 from WSIs with other diagnoses. We handpicked patches to ensure they included diverse regions of the biopsies and various cell types. Each patch includes annotations drawn by pathologists using the open source QuPath software (33) outlining the villous epithelium (150 unique annotations), crypt epithelium (759), villous enterocyte nuclei (13,853), crypt enterocyte nuclei (23,657), and IELs (4,368).

Classification training dataset: We further trained a logistic regression model to classify coeliac disease versus normal diagnoses using the IEL-to-enterocyte and villus-to-crypt ratios as input features. We ran our segmentation models on 172 WSIs (77 from coeliac disease cases and 95 normal), sourced from four different institutions. The calculated ratios were then used to train the logistic regression model. This dataset only included clinical diagnoses and no further cellular annotations. A breakdown of hospital origins of these images is provided in Table S1.

Classification test set: Finally, we used an independent test set from a source from which no training data had been included. The test set included 613 WSIs of which 88 had a coeliac disease and 525 a normal diagnosis. The WSIs were scanned on a Philips IntelliSite Ultra Fast Scanner. The patient demographic breakdown of the test set is provided in Table S2.

III. Method

The overall pipeline for our proposed method (as highlighted in Figure 1) consists of three main stages: pre-processing, semantic segmentation and coeliac disease classification.

III a. Pre-processing

We take inspiration from the work of Denholm et al. (30) to develop our pre-processing pipeline.
Tissue Masking: We used Schreiber's method (34) to distinguish tissue areas from white background and unwanted artifacts and to generate tissue masks for the WSI.
Patch Extraction: Each WSI was divided into smaller patches at 40x magnification (the highest magnification available) of size 2024x2024 using QuPath.
Stain Normalization: To reduce variations caused by different staining and scanning procedures, we applied a stain normalization process using the Macenko method (35). Stain normalisation has been shown by many studies to improve generalisation performance (36–38).

III b. Cellular Segmentation

We trained two separate sets of semantic segmentation models: villus-crypt models and IEL-enterocyte models:

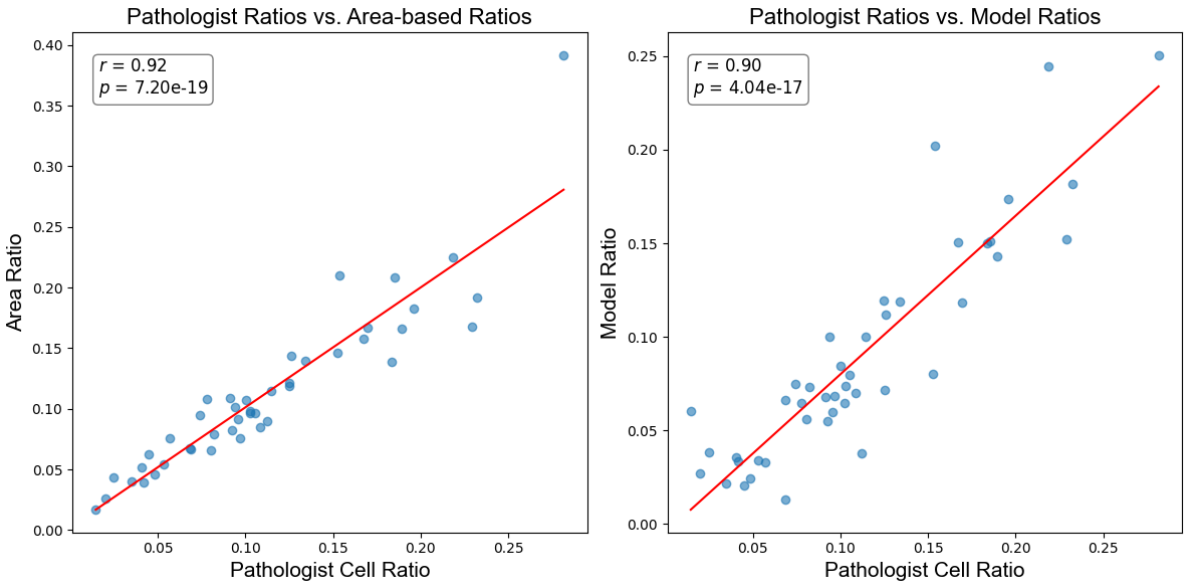

Figure 2. Comparisons of IEL-to-enterocyte ratio estimates. Left: *The IEL-to-enterocyte ratio derived from pathologists' cell annotations was compared to the ratio estimated based on the total area covered by pathologists' annotated IELs and enterocytes. Pearson correlation analysis revealed a strong correlation with an r-value of* 0.92 $(p = 7.20 \times 10^{-19})$. *The mean absolute was* 0.016 ± 0.02. ***Right:*** *The IEL-to-enterocyte ratio from pathologists' annotations was compared to the ratio estimated by the AI model on a validation dataset of 49 images. Pearson correlation analysis showed a strong correlation, with an r-value of* 0.90 $(p = 4.04 \times 10^{-17})$. *The mean absolute error was* 0.028 ± 0.019.

Villus-crypt model: we used the U-Net architecture (39) with a ResNet32 encoder (40) initialised with ImageNet pre-trained weights (41) and a final softmax layer applied on a pixel basis. We trained the models using 3-fold cross-validation for 70 epochs using the Adam optimiser with a cosine cycling learning rate scheduler (with a minimum and maximum learning rate of 1e-5 and 5e-5, respectively, updated at the end of every epoch) and using the focal loss (42). We downsized each patch by a factor of two to 1024x1024 (at 20x magnification) and applied extensive data augmentation: random horizontal flips, rotations, and shifts, were applied to introduce spatial variability, while colour jittering (p=0.2) simulated changes in brightness $[0.9,1.1]$, contrast $[0.9,1.1]$, saturation $[0.8,1.0]$, and hue $[-0.5,0.5]$. All code has been implemented in PyTorch (v1.13.1) (43).

IEL-enterocyte model: The IEL-enterocyte model focuses solely on the areas of the WSI that have already been segmented as either villi or crypts. During training we used the mask provided by the pathologist and during inference we used the output from the villus-crypt model to determine which parts of the image the models should focus on. We used the same model architecture and a similar set-up as before: we trained the models for 60 epochs and with a cycling learning rate scheduler where the minimum and maximum learning rates were 5e-5 and 5e-4, respectively. The most significant difference to the villus-crypt model was that here we split each patch into four smaller patches of size

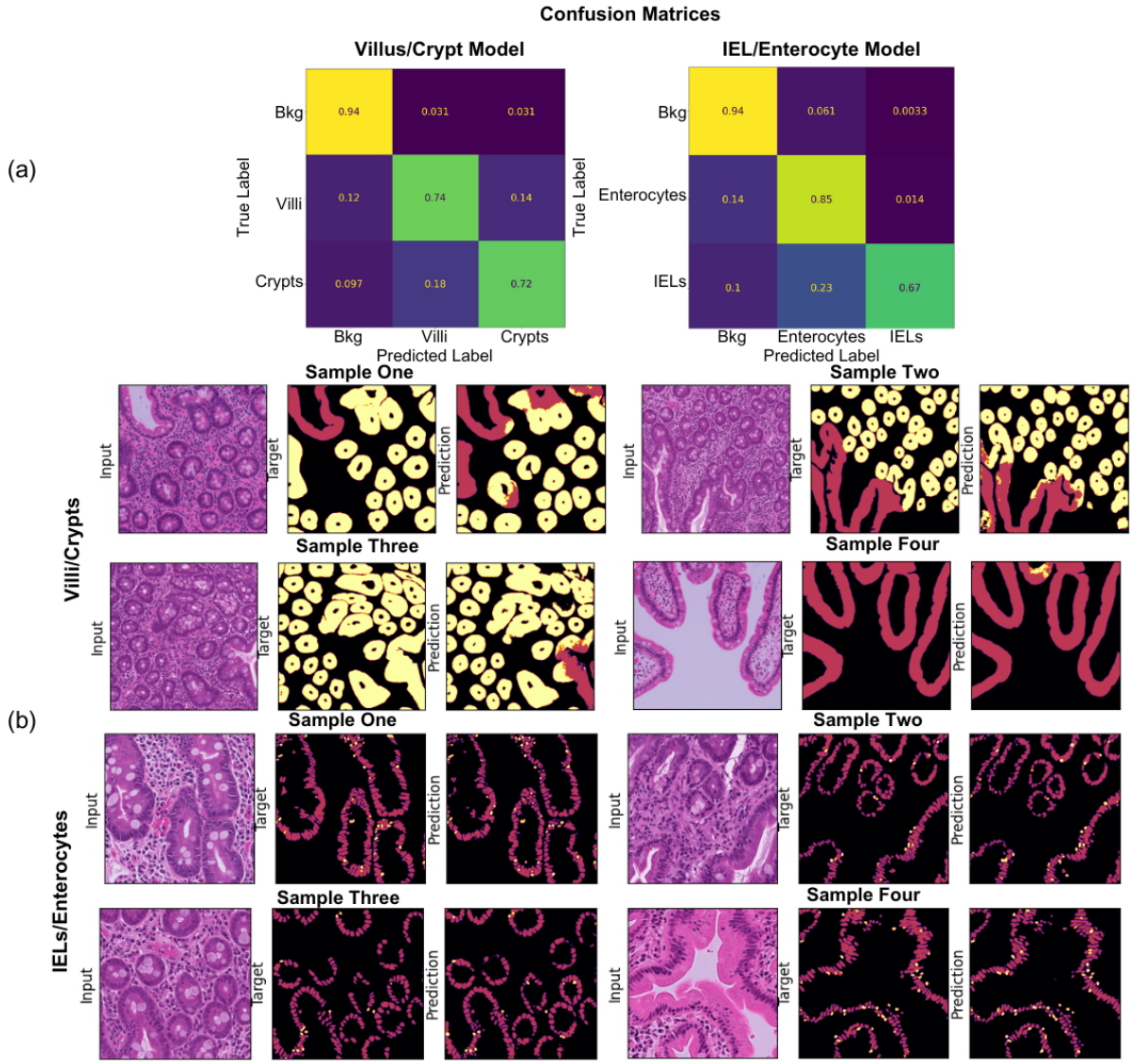

Figure 3. Validation Performance. *a) Confusion matrix showing the mean validation performance of the two segmentation models on a pixel basis, normalised per true label (i.e., per row). For example, 72% of pixels annotated as crypts by pathologists were correctly segmented as crypts by the models. The most common misclassification was labelling IEL pixels as enterocyte pixels. b) Examples of validation images for each model set. Columns 1 and 4 display the raw image patches, columns 2 and 5 show pathologists' annotations, and columns 3 and 6 show the corresponding model predictions.*

1024x1024 at 40x magnification, as a form of regularization. As IELs and enterocytes are significantly smaller than villi and crypts, a higher magnification was needed.

III c. Coeliac Disease Classification

Finally, we fit a simple logistic regression classifier that makes either a normal or coeliac disease diagnosis based on the masks produced by the two segmentation models. We

first compute the villus-to-crypt area ratio, a proxy for villous atrophy and crypt hyperplasia, by diving the number of pixels segmented as villi in the entire WSI by the number of pixels classified as crypt. Similarly, we compute the IEL-to-enterocyte ratio separately in the villi and the crypts. We then fit a simple logistic regression classifier that takes as input the three ratios and outputs a single diagnosis. Supplementary material D provides a more comprehensive analysis of the classification model.

IV. Results

We first show how accurately we can predict the IEL-to-enterocyte ratio from segmentation masks. We then summarise the validation results of our segmentation before testing our segmentation and classification models on the independent test set.

IV a. Predicting IEL-to-enterocyte ratios

As semantic segmentation masks do not specify instances of individual objects, but instead label each pixel as belonging to a type of object (e.g. an IEL), we can only estimate the number of instances of an object type (e.g. the number of IELs in a biopsy). We can predict the IEL-to-enterocyte ratio by dividing the number of pixels classified as IELs by the number of pixels classified as enterocytes in either crypts or villi whilst correcting for the different average cell sizes. As shown in Figure 2, Pearson correlation analysis showed that the ratio based on the total area covered by pathologists' annotated IELs and enterocytes correlates very highly with the true IEL-to-enterocyte ratio derived from pathologists' cell annotations ($r = 0.92, p = 7.20e^{-19}$). As pathologists do not count cells in the entire biopsy but rather in a few selected regions of interest, the mean absolute error of 0.016 ± 0.020 (which correspond to less than 2 IELs per 100 enterocytes) is not very significant. Predicting the IEL-to-enterocyte ratio based on the semantic segmentation masks is therefore justified assuming the mask is accurate.

IV b. Validation of Semantic Segmentation Models

We trained and validated both the villus-crypt models and the IEL-enterocyte models using 3-fold cross-validation on the 49 annotated 2048x2048 patches. As summarised in Table S3, the villus-crypt models segmented villi with a mean accuracy of 90%, precision (positive predictive value) of 67% and recall (sensitivity) of 80%. The same models segment crypts with a mean accuracy of 90%, precision (positive predictive value) of 78%, and recall (sensitivity) of 71%.

The IEL-enterocyte models achieve mean accuracies of 91% and 99%, precisions (positive predictive values) of 85% and 65%, and recall (sensitivity) values of 85% and 67% for enterocytes and IELs, respectively, as summarised in Table S3. We include confusion matrices and some example patches in Figure 3, thereby further visualising the models' validation performance.

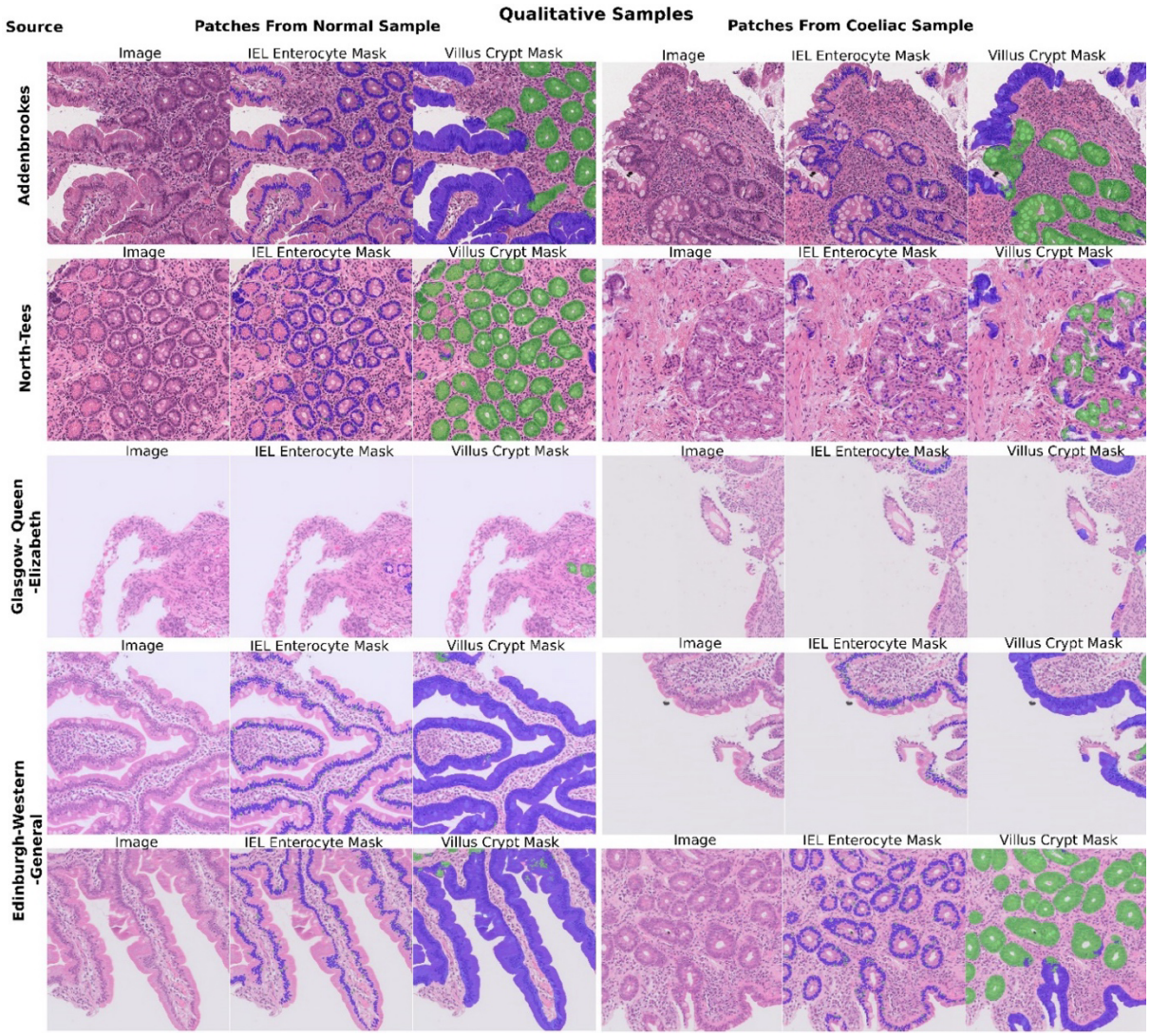

Figure 4. Sample visual outputs of segmentation models on test images: *We showcase patches from 5 coeliac disease biopsies and 5 normal biopsies, collected from 4 different hospitals. For each patch, three visualisations are provided: i) the original H&E-stained image, ii) the segmentation mask for IELs and enterocytes, and iii) the segmentation mask for villi and crypts. These outputs demonstrate the models' robustness and effectiveness across diverse sources and tissue characteristics.*

Finally, we validated how accurately our segmentation models can estimate the IEL-to-enterocyte ratio, a key feature in the pathologist's diagnosis of coeliac disease. As shown in Figure 2b, the IEL-to-enterocyte ratio estimated by the segmentation models only differs from the ratio calculated from the pathologists' manual annotations by a mean absolute value of 0.028 (which correspond to 3 IELs per 100 enterocytes). Given that the threshold indicating coeliac disease used by pathologists varies between 0.2 and 0.4 (equivalent to 20 to 40 IELs per 100 enterocytes)(44–46), and the range of pathologist's

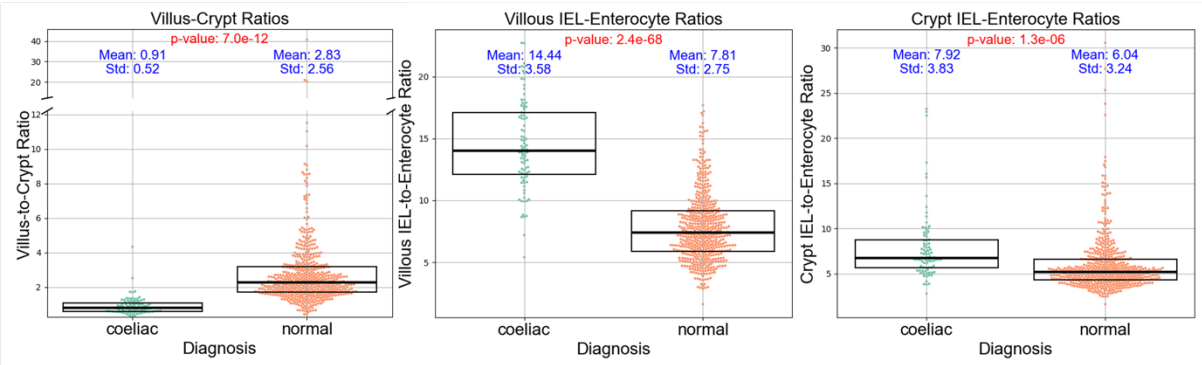

Figure 5. Ratio distributions on the test set. *We highlight the distributions of a) villus-to-crypt ratios, b) IEL-to-enterocyte ratios in the villi, and c) IEL-to-enterocyte ratios in the crypts for the normal and coeliac disease populations on the independent test data. We observed statistically significant differences for all three ratios (p values of* $7.0e^{-12}$*,* $2.4e^{-68}$*, and* $1.3e^{-6}$*, respectively). More information about the three outliers in the villus-to-crypt ratio plot can be found in appendix E.*

cell ratios across the patches spans from 0.02 to 0.28, we conclude that a mean error of 0.028 is acceptable and unlikely to be significant. The Pearson test further showed a strong correlation ($r = 0.90, p = 7.20e^{-19}$) between the pathologist's and the model's ratios. We further analyse the different IEL-to-enterocyte ratios in Appendix C.

IV c. Test of the Coeliac Disease Classification Models

We also tested our coeliac disease classification pipeline that takes as input an entire WSI, then firstly carries out the pre-processing steps described in the methods section (background/artefact removal, patch extraction, stain normalisation), secondly runs the villus-crypt segmentation model, thirdly runs the IEL-enterocyte segmentation model, fourthly, computes the villus-to-crypt ratio as well as the IEL-to-enterocyte ratios in the villi and the crypts, and fifthly runs a classifier that takes as input these three ratios and outputs a diagnosis of either "normal" or "coeliac disease".

We tested our segmentation models on a dataset comprising over 600 images from a previously unseen source to test the diagnostic accuracy and generalisation performance of our models. We visualise the output of the segmentation models on a few selected patches in Figure 4. As illustrated in Figure 5, the ratios we get for the normal and the coeliac disease populations are significantly different. The mean villus-to-crypt ratios were 0.91 ± 0.52 for the coeliac disease population and 2.83 ± 2.56 for the normal population ($p = 7.0 \times 10^{-12}$ using the independent samples t-Test), reflecting the significant level of villous blunting that can be observed in the majority of coeliac disease biopsies. Conversely, the IEL-to-enterocyte ratio in the villi is significantly higher ($p = 2.4 \times 10^{-68}$) for coeliac disease cases (14.44 ± 3.58) than it is for normal ones (7.81 ± 2.75), which matches clinical practice where pathologists use an increased IEL count in the villi as a key indication for coeliac disease. Interestingly, a statistically significant difference ($p = 1.3e^{-6}$) is observed in the crypt IEL-to-enterocyte ratio, even

though this metric is not typically considered by pathologists when diagnosing coeliac disease.

Next, we evaluated the linear regression-based classifier on the same independent test set and achieved 96% accuracy, 86% positive predictive value (precision), and 98% negative predictive value, thus demonstrating how we can make an accurate explainable coeliac disease diagnosis. Importantly, we confirmed that our overall classification process for coeliac disease, based on semantic segmentation, followed by linear regression-based classification, achieved greater than 89% accuracy for all patient groups regardless of age and sex (Figure S6).

V. Discussion

We have presented an accurate, explainable, and generalizable method for coeliac disease diagnosis in this work. We trained two sets of segmentation model to highlight villi, crypts, IELs, and enterocytes in duodenal biopsies. The segmentation masks can be reviewed by pathologists to develop trust in the model. We further showed how the model is able to estimate accurately the IEL-to-enterocyte ratio, one of the key characteristics on which pathologists base their coeliac disease diagnosis. We then demonstrated how the IEL-to-enterocyte and the villus-to-crypt ratios returned by the segmentation models are significantly different ($p<0.00001$) for the normal and coeliac disease populations. We subsequently trained a classifier that takes these ratios as input, and which gives a coeliac disease or normal diagnosis with over 94% accuracy. Unlike other previous works that aimed to train segmentation models for the diagnosis of coeliac disease, we tested our models on an independent test set, including over 600 cases from a new hospital not previously used to train the models. We thus demonstrated very strong generalisability of our models.

The work we presented marks an important step towards improving coeliac disease diagnosis for several key reasons. First, there is a global shortage of pathologists, resulting in long waiting times (47,48). Second, studies consistently report high rates of disagreement among pathologists when diagnosing coeliac disease (11–21). Third, most existing AI studies aimed at improving coeliac disease diagnosis function as "black boxes," limiting their acceptance by healthcare professionals and patients due to a lack of transparency (22,23,26–30).

Our interpretable AI approach establishes a foundation for faster, more accurate, and trustworthy coeliac disease diagnosis. Unlike pathologists, who typically estimate cell ratios based on small, selected regions of a slide, our model delivers a comprehensive, high-resolution, cell-by-cell analysis across the entirety of the biopsy, encompassing thousands or even tens of thousands of cells. To the best of our knowledge our approach is the first explainable segmentation-based AI approach for coeliac disease diagnosis that has been tested on a comprehensive independent test set from a different hospital to the training and validation datasets.

Future work could extend the segmentation models to different types of cells, such as goblet cells, Paneth cells, or Brunner's glands. Instance segmentation models may also

return more accurate cell counts. The main limitation of this work is the lack of a perfect ground truth due to the imperfect nature of pathologists' coeliac disease diagnosis. We hope that, in the future, our work can improve this situation, by providing more reproducible diagnosis of duodenal biopsies.

Author's Contribution

F.J., R.B., J.D., and J.R.D. developed the underlying methodology. E.S. conceived and set up the overall study. F.J. and R.B. drafted the manuscript. V.S. and D.E. created the cellular annotations for the training and validation dataset under the supervision of M.J.A.; J.D., B.S., V.S., S.C.E., and E.S. set up the annotation pipeline. All authors contributed to and had the opportunity to review and correct drafts of the manuscript.

Acknowledgements

We would like to thank and acknowledge Graham Snudden for organisational support.

Declaration of Interest

The authors declare the following financial interests/personal relationships which may be considered as potential competing interests: The following authors are shareholders in Lyzeum Ltd: F.J., J.D., M.J. A., and E.S.

Funding

This work has been supported by Coeliac UK, Innovate UK (grant INOV03-- 19 to ES), NIHR (grant NIHR205502) and the Cambridge Centre for Data-Driven Discovery (C2D3).

Ethics Approval

This study involves human participants and was approved. All slide scans (and accompanying fully anonymised patient data) were obtained with full ethical approval (IRAS: 162057; PI: Dr E Soilleux). Organisation: South Central – Oxford A (formally known as Oxfordshire Research Ethics Committee A).

Data Availability

The datasets of WSIs analysed during this current study have not publicly available due to the large size of the WSIs and no patient agreements.

References:

1. Berge-Henegouwen GPV, Mulder CJJ. Pioneer in the gluten free diet: Willem-Karel Dicke 1905-1962, over 50 years of gluten free diet. Gut. 1993 Nov;34(11):1473–5.

2. Guandalini S, Assiri A. Celiac disease: A review. JAMA Pediatr. 2014 Mar;168(3):272–8.

3. Singh P, Arora A, Strand TA, Leffler DA, Catassi C, Green PH, et al. Global prevalence of celiac disease: systematic review and meta-analysis. Clin Gastroenterol Hepatol. 2018;16(6):823–36.

4. Caio G, Volta U, Sapone A, Leffler DA, De Giorgio R, Catassi C, et al. Celiac disease: a comprehensive current review. BMC Med. 2019;17:1–20.

5. Haines ML, Anderson RP, Gibson PR. Systematic review: the evidence base for long-term management of coeliac disease. Aliment Pharmacol Ther. 2008 Nov;28(9):1042–66.

6. Silano M, Volta U, Mecchia AM, Dessì M, Di Benedetto R, De Vincenzi M. Delayed diagnosis of coeliac disease increases cancer risk. BMC Gastroenterol. 2007 Dec;7(1):8.

7. Caio G, Volta U, Sapone A, Leffler DA, De Giorgio R, Catassi C, et al. Celiac disease: a comprehensive current review. BMC Med. 2019 Dec;17(1):142.

8. Ludvigsson JF, Bai JC, Biagi F, Card TR, Ciacci C, Ciclitira PJ, et al. Diagnosis and management of adult coeliac disease: guidelines from the British Society of Gastroenterology. Gut. 2014;63(8):1210–28.

9. Health NI for, Britain) CE (Great. Coeliac disease: recognition, assessment and management. National Institute for Health and Care Excellence, Internal Clinical …; 2015.

10. Nasser J, Jansson-Knodell C, Rubio-Tapia A. Celiac disease: Who should I test, and how? Cleve Clin J Med. 2023;90(6):349–52.

11. Villanacci V, Magazzù G, Pellegrino S, Gambarotti M, Sferlazzas C, Tuccari G, et al. Comparison of the Marsh–Oberhuber classification with a new grading system in identifying patients with latent celiac disease. Minerva Gastroenterol Dietol. 2010 Dec;56(4):371–5.

12. Corazza GR, Villanacci V, Zambelli C, Milione M, Luinetti O, Vindigni C, et al. Comparison of the Interobserver Reproducibility With Different Histologic Criteria Used in Celiac Disease. Clin Gastroenterol Hepatol. 2007 Jul;5(7):838–43.

13. Arguelles-Grande C, Tennyson CA, Lewis SK, Green PHR, Bhagat G. Variability in small bowel histopathology reporting between different pathology practice settings: Impact on the diagnosis of coeliac disease. J Clin Pathol. 2012 Mar;65(3):242–7.

14. Niveloni SI, Cabanne AM, Vázquez H, Sugai E, Galich M, Smecuol E, et al. 1042 “Experts” Assess the Accuracy of Celiac Disease Diagnosis Performed in the Community Setting. Gastroenterology. 2012 May;142(5):S-183.

15. Weile B, Hansen BF, Hägerstrand I, Hansen JPH, Krasilnikoff PA. Interobserver variation in diagnosing coeliac disease. A joint study by Danish and Swedish pathologists. APMIS. 2000 Jan;108(5):380–4.

16. Mubarak A, Nikkels P, Houwen R, Kate FT. Reproducibility of the histological diagnosis of celiac disease. Scand J Gastroenterol. 2011 Sep;46(9):1065–73.

17. Bilkhoo HK, Ducruet T, Marchand V, Deslandres C, Djemli A, Soglio DD, et al. Revisiting pathological criteria for earlier diagnosis of coeliac disease. J Pediatr Gastroenterol Nutr. 2016 May;62(5):734–8.

18. Ghanghoria S, Sharma S, Jain P. Celiac Disease: Comparison of Oberhuber Classification and Corazza-Villanacci classification. Ann Pathol Lab Med. 2019 Mar;6(3):A135-140.

19. Montén C, Bjelkenkrantz K, Gudjonsdottir AH, Browaldh L, Arnell H, Naluai ÅT, et al. Validity of histology for the diagnosis of paediatric coeliac disease: A Swedish multicentre study. Scand J Gastroenterol. 2016 Apr;51(4):427–33.

20. Webb C, Halvarsson B, Norström F, Myléus A, Carlsson A, Danielsson L, et al. Accuracy in celiac disease diagnostics by controlling the small-bowel biopsy process. J Pediatr Gastroenterol Nutr. 2011 May;52(5):549–53.

21. Denholm J, Schreiber BA, Jaeckle F, Wicks MN, Benbow EW, Bracey TS, et al. CD, or not CD, that is the question: a digital interobserver agreement study in coeliac disease. BMJ Open Gastroenterol. 2024;11(1):e001252.

22. Wei JW, Wei JW, Jackson CR, Ren B, Suriawinata AA, Hassanpour S. Automated Detection of Celiac Disease on Duodenal Biopsy Slides: A Deep Learning Approach. J Pathol Inform. 2019 Jan;10(1):7.

23. Sali R, Ehsan L, Kowsari K, Khan M, Moskaluk CA, Syed S, et al. CeliacNet: Celiac Disease Severity Diagnosis on Duodenal Histopathological Images Using Deep Residual Networks. Proc - 2019 IEEE Int Conf Bioinforma Biomed BIBM 2019. 2019 Nov;962–7.

24. Marsh MN. Gluten, major histocompatibility complex, and the small intestine: a molecular and immunobiologic approach to the spectrum of gluten sensitivity (‘celiac sprue’). Gastroenterology. 1992;102(1):330–54.

25. Oberhuber G, Granditsch G, Vogelsang H. The histopathology of coeliac disease: time for a standardized report scheme for pathologists. Eur J Gastroenterol Hepatol. 1999;11(10):1185.

26. Syed S, Al-Boni M, Khan MN, Sadiq K, Iqbal NT, Moskaluk CA, et al. Assessment of machine learning detection of environmental enteropathy and celiac disease in children. JAMA Netw Open. 2019;2(6):e195822–e195822.

27. Koh JEW, De Michele S, Sudarshan VK, Jahmunah V, Ciaccio EJ, Ooi CP, et al. Automated interpretation of biopsy images for the detection of celiac disease using a machine learning approach. Comput Methods Programs Biomed. 2021;203:106010.

28. Kowsari K, Sali R, Ehsan L, Adorno W, Ali A, Moore S, et al. Hmic: Hierarchical medical image classification, a deep learning approach. Information. 2020;11(6):318.

29. Tabacchi ME, Tegolo D, Cascio D, Valenti C, Sorce S, Gentile V, et al. A fuzzy-based clinical decision support system for coeliac disease. IEEE Access. 2022;10:102223–36.

30. Denholm J, Schreiber BA, Evans SC, Crook OM, Sharma A, Watson JL, et al. Multiple-instance-learning-based detection of coeliac disease in histological whole-slide images. J Pathol Inform. 2022;13:100151.

31. Gruver AM, Lu H, Zhao X, Fulford AD, Soper MD, Ballard D, et al. Pathologist-trained machine learning classifiers developed to quantitate celiac disease features differentiate endoscopic biopsies according to modified marsh score and dietary intervention response. Diagn Pathol. 2023 Nov 11;18(1):122.

32. Griffin M, Gruver A, Shah C, Wani Q, Fahy D, Khosla A, et al. Fully automated histological classification of cell types and tissue regions of celiac disease is feasible and correlates with the Marsh score. medRxiv. 2023;2023–12.

33. Bankhead P, Loughrey MB, Fernández JA, Dombrowski Y, McArt DG, Dunne PD, et al. QuPath: Open source software for digital pathology image analysis. Sci Rep. 2017 Dec;7(1):1–7.

34. Schreiber BA, Denholm J, Jaeckle F, Arends MJ, Branson KM, Schönlieb CB, et al. Rapid artefact removal and H&E-stained tissue segmentation. Sci Rep. 2024;14(1):309.

35. Macenko M, Niethammer M, Marron JS, Borland D, Woosley JT, Guan X, et al. A method for normalizing histology slides for quantitative analysis. In: 2009 IEEE international symposium on biomedical imaging: from nano to macro. IEEE; 2009. p. 1107–10.

36. Schreiber BA, Denholm J, Gilbey JD, Schönlieb CB, Soilleux EJ. Stain normalization gives greater Generalizability than stain Jittering in neural network training for the classification of Coeliac disease in Duodenal biopsy whole slide images. J Pathol Inform. 2023;14:100324.

37. Ciompi F, Geessink O, Bejnordi BE, De Souza GS, Baidoshvili A, Litjens G, et al. The importance of stain normalization in colorectal tissue classification with convolutional networks. In: 2017 IEEE 14th International Symposium on Biomedical Imaging (ISBI 2017) [Internet]. IEEE; 2017 [cited 2024 Nov 15]. p. 160–3. Available from: https://ieeexplore.ieee.org/abstract/document/7950492/?casa_token=VnfAVGMIPJYAAAAA:4k3tpZHTrJqpa7HXaUEJQVNuBPGpLk7AVh_1FyP-7oajIRoV4ZEMx2tOgztD7Zy4fGpjkWqKgA

38. Salvi M, Caputo A, Balmativola D, Scotto M, Pennisi O, Michielli N, et al. Impact of stain normalization on pathologist assessment of prostate cancer: a comparative study. Cancers. 2023;15(5):1503.

39. Ronneberger O, Fischer P, Brox T. U-Net: Convolutional Networks for Biomedical Image Segmentation. In: Navab N, Hornegger J, Wells WM, Frangi AF, editors. Medical Image Computing and Computer-Assisted Intervention – MICCAI 2015 [Internet]. Cham: Springer International Publishing; 2015 [cited 2024 Nov 15]. p. 234–41. (Lecture Notes in

Computer Science; vol. 9351). Available from: http://link.springer.com/10.1007/978-3-319-24574-4_28

40. He K, Zhang X, Ren S, Sun J. Deep residual learning for image recognition. In: Proceedings of the IEEE Computer Society Conference on Computer Vision and Pattern Recognition. IEEE Computer Society; 2016. p. 770–8.

41. Deng J, Dong W, Socher R, Li LJ, Li K, Fei-Fei L. ImageNet: A large-scale hierarchical image database. In Institute of Electrical and Electronics Engineers (IEEE); 2010. p. 248–55.

42. Ross TY, Dollár G. Focal loss for dense object detection. In: proceedings of the IEEE conference on computer vision and pattern recognition [Internet]. 2017 [cited 2024 Nov 15]. p. 2980–8. Available from: http://openaccess.thecvf.com/content_ICCV_2017/papers/Lin_Focal_Loss_for_ICCV_2017_paper

43. Paszke A, Gross S, Massa F, Lerer A, Bradbury J, Chanan G, et al. Pytorch: An imperative style, high-performance deep learning library. Adv Neural Inf Process Syst. 2019;32.

44. Walker MM, Murray JA, Ronkainen J, Aro P, Storskrubb T, D'Amato M, et al. Detection of celiac disease and lymphocytic enteropathy by parallel serology and histopathology in a population-based study. Gastroenterology. 2010;139(1):112–9.

45. Mahadeva S, Wyatt JI, Howdle PD. Is a raised intraepithelial lymphocyte count with normal duodenal villous architecture clinically relevant? J Clin Pathol. 2002;55(6):424–8.

46. Hayat M, Cairns A, Dixon MF, O'Mahony S. Quantitation of intraepithelial lymphocytes in human duodenum: what is normal? J Clin Pathol. 2002;55(5):393–4.

47. Robboy SJ, Weintraub S, Horvath AE, Jensen BW, Alexander CB, Fody EP, et al. Pathologist workforce in the United States: I. Development of a predictive model to examine factors influencing supply. Arch Pathol Lab Med. 2013 Dec;137(12):1723–32.

48. Adesina A, Chumba D, Nelson AM, Orem J, Roberts DJ, Wabinga H, et al. Improvement of pathology in sub-Saharan Africa. Lancet Oncol. 2013 Apr;14(4):e152–7.